Nonlinear Dynamics and Performance Enhancement of Multi-stable Wideband Energy Harvesting: Theoretical Analysis

IOP Conf. Series: Materials Science and Engineering **531** (2019) 012040 doi:10.1088/1757-899X/531/1/012040

Nonlinear Dynamics and Performance Enhancement of Multi-stable Wideband Energy Harvesting: Theoretical Analysis

C Wang[1], **X Yang**[1] **and S K Lai**[1,2,*]

[1] Department of Civil and Environmental Engineering, The Hong Kong Polytechnic University, Hung Hom, Kowloon, Hong Kong, P.R. China
[2] The Hong Kong Polytechnic University Shenzhen Research Institute, Shenzhen, P.R. China

Abstract. A new multi-stable wideband harvester is proposed to increase the power density of energy harvesting under wide-bandwidth and low-frequency operations. This harvester can possess with an arbitrary multi-stable state by combining the nonlinearities of stopper-engaged cantilevers and magnetic forces. The harvesting efficiency can be enhanced by interwell oscillations and the global amplitude of the harvester is restricted by the cantilever-stopper engagement. An electromechanical coupling model of the proposed harvester is established to describe its dynamic characteristics. To explore the influence of potential well configurations on a multi-stable energy harvesting, the proposed harvester with four typical potential well configurations is considered while its equivalent nonlinear restoring force can be experimentally identified. The dynamic characteristics of these four configurations at different levels of a harmonic excitation will be explored by both numerical and experimental methods. It is expected that a multiple-well potential with non-uniform depths and shallower outer wells is much more suitable for the proposed system when the external excitation exceeds a critical intensity.

Keywords: Multi-stable state, Energy harvesting system, Magnetoelasticity, Interwell motion

1. Introduction

Recently, the application of energy harvesting from ambient vibrations via piezoelectric transducers has been actively undertaken in powering wireless sensors and MEMS [1–3]. For mechanical vibration energy harvesters, the maximum energy transduction is usually obtained when they operate at a resonant effect. It is essential to restrict the resonant frequencies of such energy harvesters in the bandwidth of ambient vibrations. However, ambient vibrations around us are typically governed by a broadband spectrum, and they are usually dominant at very low frequencies (typically 1–30 Hz) [4, 5]. Conventional linear energy harvesters, with a narrow bandwidth, are thus incapable of working efficiently.

Facing this issue, it encourages the exploration of new methods to expand the operation bandwidth at low frequencies, e.g., oscillator arrays and frequency-tuning method [6, 7]. Another significant enhancement for a broadband performance is achieved by introducing nonlinearities to linear harvesters. Accordingly, nonlinear harvesters such as mono-stable harvesters [8, 9] and bi-stable harvesters [10, 11] have been intensively investigated for improving the efficiency of energy conversion over a low-frequency broadband. Particularly, the use of bi-stable energy harvesters has received much attention

*Corresponding author. E-mail: sk.lai@polyu.edu.hk (S.K. Lai)

because of their high power output when the potential escape phenomenon (inducing high-energy interwell motions) occurs. However, it has been recognized that the potential energy barriers in bi-stable energy harvesters can inhibit the occurrence of interwell motions and make it difficult to maintain the high-energy interwell motion under a low excitation level [12]. To improve the performance of such harvesters under a low excitation level, multi-stable energy harvesters (MEHs) with tri-stability [13–17] have been developed. With the presence of extra static equilibrium states and shallow potential wells, the tri-stable approach is beneficial to harness energy from wideband and low-intensity vibration sources, and its frequency threshold for interwell oscillations is lower than the bi-stable one.

Since the ability of nonlinearities can extend the bandwidth of resonant frequencies, not changing them directly, low fundamental frequency oscillators are still needed in MEHs for the sake of low frequency harvesting. However, most existing MEHs can only enhance the voltage generation by enlarging the amplitude of oscillation [11–14]. This makes the MEHs show the same performance in power density as the conventional low resonant frequency counterpart in essence. Unfortunately, low-frequency energy harvesters generally suffer from the problem of low-power density. One reason is the power generated by an energy harvester decreases cubically with the frequency of applied vibration [18]. Besides, for a given mass, a large mechanical displacement is required to permit the resonance of increasingly compliant springs at lower frequencies, thereby resulting in an extra space consumption [19]. Making use of conventional low resonant frequency energy harvesters, the power density can be improved by impact/engagement-based methods, such as a mechanical frequency up-conversion technology [19–23]. These methods employ a low-frequency oscillator to absorb energy from environmental vibrations and transfer the absorbed energy to high power output during a short period of time under an impact/engagement vibration with high frequencies. The performance of such methods depends on the amplitude of impact/engagement behavior [20, 21].

In this study, the concept of a new piezoelectric wideband harvester, with an arbitrary multi-stability induced by the combination of magnetoelasticity and cantilever-stopper engagement, is proposed. The aim of this coupling effect is to improve the power density of this harvester by enhancing the energy efficiency through inter-well oscillations and restricting a large global amplitude of the tip mass through the cantilever-stopper engagement.

2. Principle and mechanism of the new multi-stable wideband harvester

To improve the power density of broadband harvesters at low frequencies, a multi-stable oscillator that can possess an arbitrary multi-stability is introduced in this section. This multi-stable oscillator consists of two parts, i.e., a piecewise linear spring and three magnets that can generate magnetoelasticity. In the previous study, Wang and his co-workers [23, 24] have integrated the magnetic nonlinearity and mechanical piecewise-linearity to construct a frequency up-converted energy harvester with a quintuple-well potential. Here, we further discuss the working principle of these two parts and its mechanism to achieve an arbitrary multi-stable state.

2.1. Piecewise linear springs based on a cantilever-stopper engagement

In the present multi-stable oscillator, the piecewise-linear spring is employed to increase strains in the piezoelectric transducer and restrict a large displacement of the proof mass. It can be physically realized by adding symmetric stoppers to a conventional linear oscillator, e.g., a cantilever beam, as shown in Figure 1(a). The piecewise-defined linear restoring force of such a spring is plotted in Figure 1(b). There is a low initial stiffness k_1 to couple low-frequency external excitations. As the deflection z increases, the beam firstly engages the stopper 1 when $|z| \geq z_1$ and changes the effective length of the beam from l to $(l-l_1)$, while the corresponding stiffness of oscillator increases from k_1 to k_2. As the deflection z further increases, the beam engages the stopper 2 when $|z| \geq z_2$ and changes the effective length of the beam from $(l-l_1)$ to $(l-l_2)$ with increasing the stiffness from k_2 to k_3. This architecture can restrict the deflection of the cantilever beam and form a large-strain region around the engagement point. According to the classical beam theory and the superposition principle of displacements [23, 24], we have

$$d_1 = \frac{F_1 l_1^3}{3EI} + \frac{F_2 l_1^2}{6EI}(3l_2 - l_1) + \frac{F_3 l_1^2}{6EI}(3l - l_1) \tag{1a}$$

$$d_2 = \frac{F_1 l_1^2}{6EI}(3l_2 - l_1) + \frac{F_2 l_2^3}{3EI} + \frac{F_3 l_2^2}{6EI}(3l - l_2) \tag{1b}$$

$$z = \frac{F_1 l_1^2}{6EI}(3l - l_1) + \frac{F_2 l_2^2}{6EI}(3l - l_2) + \frac{F_3 l^3}{3EI} \tag{1c}$$

where d_1 and d_2 are the gap distances of the cantilever-stoppers, F_1 and F_2 are the forces on the stoppers during engagement, F_3 is the tip force, z is the deflection of the cantilever tip, and EI is the bending modulus of the cantilever beam. The engagement positions z_1 and z_2 can be written as

$$z_1 = \frac{2d_1 l^3}{l_1^2(3l - l_1)}$$

$$z_2 = \frac{-d_2(l - l_1)^2(4l - l_1)l_1 + d_1(l - l_2)\left(-2l^2(l_1 - 3l_2) + l_1 l_2^2 - l l_2(2l_1 + 3l_2)\right)}{l_1(l_1 - l_2)\left(-3ll_1 + l_2^2 + 6ll_2 - 2l_1 l_2 - 2l_2^2\right)} \tag{2}$$

Since the stoppers attached on this spring can only offer a one-way force, the stopper 1 is separated from the cantilever beam, and the stopper 2 can engage the beam when the tip deflection z exceeds a critical value, i.e., z_3. Based on Eq. (1), the critical value z_3 is derived as follows

$$z_3 = \frac{d_1 l_2^3(4l^2 - 5ll_2 + l_2^2) + d_2 l_1^2\left(2l^2(l_1 - 3l_2) - l_1 l_2^2 + l l_2(2l_1 + 3l_2)\right)}{3l_1^2(l_1 - l_2)l_2^2} \tag{3}$$

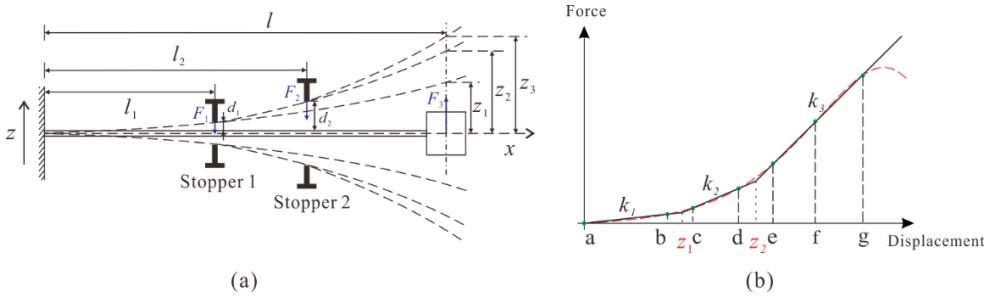

(a) (b)

Figure 1. (a) Schematic drawing of a cantilever beam structure with stoppers; (b) Restoring force.

Since the strain of the cantilever beam is proportional to its curvature, the maximum curvature of the cantilever beam is investigated herein. Using the Euler-Bernoulli equation and substituting Eq. (1) into it, the curvatures $R_1(z)$, $R_2(z)$ and $R_3(z)$ correspond to the position of the cantilever root, the engagement position of the stopper 1 and the engagement position of the stopper 2, respectively. They are given by

$$R_1(z) = \begin{cases} -\dfrac{6\left(d_1 l(-2l + l_1) + l_1^2 z\right)}{l_1^2\left(4l^2 - 5ll_1 + l_1^2\right)} & z_1 < |z| \le z_2 \\ \dfrac{3\left(-d_2 l_1^2(l - l_1)(2l - l_1 - l_2) - d_1 l_2(l - l_2)\left(2l(l_1 - 2l_2) + l_2(l_1 + l_2)\right) + l_1^2(l_1 - l_2)^2 z\right)}{l_1^2(l - l_2)(l_1 - l_2)\left(l(l_1 - 4l_2) + l_2(2l_1 + l_2)\right)} & z_2 < |z| < z_3 \\ -\dfrac{6\left(d_2 l(-2l + l_2) + l_2^2 z\right)}{l_2^2\left(4l^2 - 5ll_2 + l_2^2\right)} & |z| \ge z_3 \end{cases} \tag{4}$$

$$R_2(z)=\begin{cases}\dfrac{6\left(d_1\left(-3l+l_1\right)+2l_1z\right)}{\left(l-l_1\right)\left(4l-l_1\right)l_1} & z_1<|z|<z_2\\ \dfrac{6\left(d_2l_1\left(-l+l_1\right)\left(-2l+l_1+l_2\right)+d_1\left(l-l_2\right)\left(l\left(l_1-3l_2\right)+2l_1l_2\right)-l_1\left(l_1-l_2\right)^2z\right)}{l_1\left(l-l_2\right)\left(l_1-l_2\right)\left(l\left(l_1-4l_2\right)+l_2\left(2l_1+l_2\right)\right)} & z_2\le|z|<z_3\\ -\dfrac{6\left(d_2\left(2l^2\left(l_1-l_2\right)-l_1l_2^2+ll_2\left(2l_1+l_2\right)\right)+l_2^2\left(-3l_1+l_2\right)z\right)}{l_2^3\left(4l^2-5ll_2+l_2^2\right)} & |z|\ge z_3\end{cases} \quad (5)$$

$$R_3(z)=\begin{cases}-\dfrac{6\left(l-l_2\right)\left(3d_1l-d_1l_1-2l_1z\right)}{\left(l-l_1\right)^2\left(4l-l_1\right)l_1} & z_1<|z|<z_2\\ \dfrac{3\left(3d_1\left(l-l_2\right)l_2^2+d_2l_1\left(-l_1^2+3l\left(l_1-2l_2\right)+2l_1l_2+2l_2^2\right)+l_1\left(l_1-4l_2\right)\left(l_1-l_2\right)z\right)}{l_1\left(l-l_2\right)\left(l_1-l_2\right)\left(l\left(l_1-4l_2\right)+l_2\left(2l_1+l_2\right)\right)} & z_2\le|z|<z_3\\ \dfrac{6\left(d_2\left(-3l+l_2\right)+2l_2z\right)}{\left(l-l_2\right)\left(4l-l_2\right)l_2} & |z|\ge z_3\end{cases} \quad (6)$$

Figure 2(a) shows the variation of $R_1(z)$, $R_2(z)$ and $R_3(z)$ with the tip deflection z in the case of l = 138 mm, l_1 = 80 mm, l_2 = 103 mm, d_1 = 1.76 mm and d_2 = 3.6 mm. When $z > z_1$, the stopper 1 starts to engage the cantilever. The curvature $R_2(z)$ increases rapidly with increasing the deflection while the curvature $R_1(z)$ decreases gradually. When $z > z_2$, the stopper 2 starts to engage the cantilever with a high curvature that appears at their engagement position, while the curvature $R_2(z)$ decreases slightly in the range of z_2-z_3. As the tip deflection z exceeds z_3, the curvatures at the engagement positions of both stoppers increase rapidly, while the curvature at the cantilever root, $R_1(z)$, decreases below zero. In general, the curvature of the cantilever-stopper engagement-based oscillator starts to exceed the curvature of a conventional cantilever beam when the tip deflection z exceeds z_2. This advantage will further expand when the tip deflection z exceeds z_3. In addition, the curvature near the cantilever tip will decrease below zero and form a negative curvature region (Figure 2(b)) when the tip deflection z is sufficiently large. This may have an adverse effect on the performance of energy harvesting if the piezoelectric transducer is continuous on the boundary of the negative curvature region. In this work, the piezoelectric layer is removed from the negative curvature region.

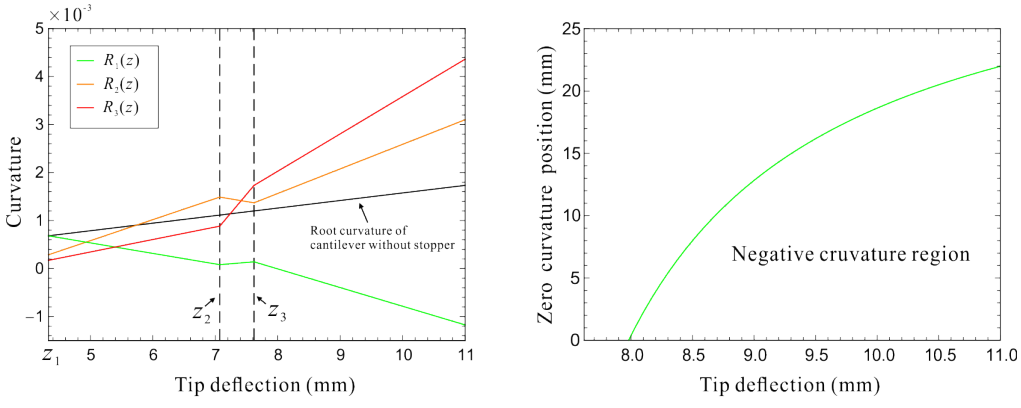

Figure 2. (a) Variation of curvatures with the tip deflection at various positions of the cantilever beam; (b) Zero curvature position on the cantilever beam varies with the tip deflection, where the zero coordinate represents the position of cantilever's fixed end.

2.2. Magnetic configurations and the formation mechanism of multi-stability

Since the large-curvature region only appears when the cantilever-stopper engagement occurs, a magnetic force F_m (its counter-force is shown by the imaginary line in Figure 1(b)) is introduced to enlarge the tip deflection during engagement. This magnetic force can soften the cantilever beam and allow the restoring force of the oscillator to have multiple zero points, e.g., positions a-g shown in Figure 1(b), which correspond to stable or unstable equilibrium positions. Then, a multi-stable oscillator can be formed. By adding or subtracting stoppers and adjusting its positions, such a multi-stable oscillator can demonstrate different multi-stable behavior.

To consider the magnetic force mentioned above, the interaction of three permanent magnets is investigated here. Figure 3(a) shows the configuration of these magnets. In the multi-stable oscillator, two fixed magnets B and C can behave attraction or repulsion on the magnet A. According to different arrangements of such magnet poles, the configurations considered here can be classified into four types (see Figures 3(b) and 3(c): (I) $\mathbf{m}_{A1}$, $\mathbf{m}_{B1}$, $\mathbf{m}_{C1}$; (II) $\mathbf{m}_{A1}$, $\mathbf{m}_{B2}$, $\mathbf{m}_{C2}$; (III) $\mathbf{m}_{A2}$, $\mathbf{m}_{B3}$, $\mathbf{m}_{C3}$; (IV) $\mathbf{m}_{A2}$, $\mathbf{m}_{B4}$, $\mathbf{m}_{C4}$. Among them, types I and IV are widely used in tri-stable energy harvesters [13–17]. For analysis, the point dipole approximation [25] is adopted to model the magnet force. In terms of a vector form, the centers of the magnets B and C to the center of the magnet A can be written as

$$\begin{aligned}\mathbf{r}_{BA} &= -h\cdot\mathbf{i} + (z+\frac{d}{2})\cdot\mathbf{j}\\ \mathbf{r}_{CA} &= -h\cdot\mathbf{i} + (z-\frac{d}{2})\cdot\mathbf{j}\end{aligned} \tag{7}$$

where $\mathbf{i}$ is the unit vector vertical to $z(t)$ and $\mathbf{j}$ is the unit vector parallel to $z(t)$.

Assume that the magnetization of two fixed magnets is uniform. Then, the magnetic flux density induced by the magnets B and C at point A is [23]

$$\mathbf{B}_A = -\frac{\mu_0}{4\pi}\nabla\frac{\mathbf{m}_B\cdot\mathbf{r}_{BA}}{|\mathbf{r}_{BA}|^3} - \frac{\mu_0}{4\pi}\nabla\frac{\mathbf{m}_C\cdot\mathbf{r}_{CA}}{|\mathbf{r}_{CA}|^3} \tag{8}$$

where $\mu_0 = 4\pi\times10^{-7}\,\mathrm{H/m}$ is permeability of vacuum; $\mathbf{m}_B$ and $\mathbf{m}_C$ are the magnetic moments of the point dipoles B and C, respectively. The potential energy of the magnetic force can be expressed as

$$U_m(Z) = -\mathbf{m}_A\cdot\mathbf{B}_A = \frac{\mu_0}{4\pi}\mathbf{m}_A\cdot\left[\left(\frac{\mathbf{m}_B}{|\mathbf{r}_{BA}|^3} - \frac{(\mathbf{m}_B\cdot\mathbf{r}_{BA})\cdot3\mathbf{r}_{BA}}{|\mathbf{r}_{BA}|^5}\right) + \left(\frac{\mathbf{m}_C}{|\mathbf{r}_{CA}|^3} - \frac{(\mathbf{m}_C\cdot\mathbf{r}_{CA})\cdot3\mathbf{r}_{CA}}{|\mathbf{r}_{CA}|^5}\right)\right] \tag{9}$$

where $\mathbf{m}_A$ is the magnetic moment of the point dipole A. Then, the magnetic force can be derived as

$$F_m(Z) = \frac{\partial U_m(Z)}{\partial Z} \tag{10}$$

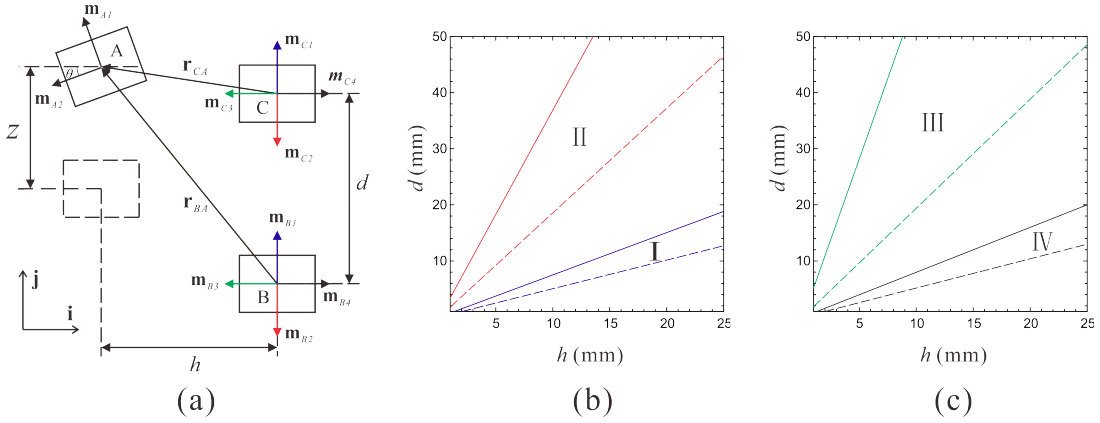

Figure 3. Forming conditions of a multi-stable performance: (a) magnet configurations; and (b)-(c) the parameter regions of multi-stability under various configurations.

For the existence of multiple equilibrium positions in a multi-stable oscillator, the second derivative of the magnetic force on the magnet A should be positive at the zero position, i.e., $F_m(0) > 0$. Besides, the magnetic force on the magnet A can soften the cantilever, i.e., $F_m(0) \le 0$. Based on these two restrictions, the parameter regions, which satisfy the forming conditions of multi-stable behavior for the configurations I, II, III and IV, can be obtained, as shown in Figures 3(b) and 3(c). Here, we consider $|\mathbf{m}_A|$=0.299 A m^2 and $|\mathbf{m}_B|$=$|\mathbf{m}_C|$=0.955 A m^2. It is obvious that the configurations II and III have a larger parameter region than that of the configurations I and IV. Therefore, the presence of multi-stable behavior in those configurations can be realized more easily. In this work, the configuration II is used for fabricating a multi-stable oscillator.

3. Conclusions

In this work, a theoretical analysis for the newly proposed piezoelectric wideband harvester that can possess any multiple stabilities induced by combined nonlinearities is presented. The formation mechanism of the corresponding parameter regions for different magnet configurations is illustrated. The electromechanical coupling model of MEHs is established to describe its dynamic characteristics. The equivalent nonlinear restoring force of four MEHs with different potential wells can be experimentally identified as a piecewise polynomial. It is expected that a multiple-well potential with non-uniform depths and shallower outer wells is much more suitable for the proposed system. On the basis of this new energy harvester model, experimental and numerical works are being conducted in progress to demonstrate its working efficiency.

Acknowledgements

The work described in this paper was supported by the Early Career Scheme from the Research Grants Council of the Hong Kong Special Administrative Region (Project No.: PolyU 252026/16E).

References

[1] Daqaq M F, Masana R, Erturk A and Quinn D D 2014 On the Role of Nonlinearities in Vibratory Energy Harvesting: A Critical Review and Discussion *Appl. Mech. Rev.* **66** 040801
[2] De Paula A S, Inman D J and Savi M A 2015 Energy harvesting in a nonlinear piezomagneticoelastic beam subjected to random excitation *Mech. Syst. Signal Pr.* **54** 405–16
[3] Erturk A and Inman D J 2011 Piezoelectric Energy Harvesting (New Jersey: John Wiley)
[4] Roundy S, Wright P K and Rabaey J 2003 A study of low level vibrations as a power source for wireless sensor nodes *Comput. Commun.* **26** 1131–44
[5] Ylli K, Hoffmann D, Willmann A, Becker P, Folkmer B and Manoli Y 2015 Energy harvesting from human motion: exploiting swing and shock excitations *Smart. Mater. Struct.* **24** 025029
[6] Tang L, Yang Y and Soh C K 2010 Toward broadband vibration-based energy harvesting *J. Intell. Mater. Syst. Struct.* **21** 1867–97
[7] Twiefel J and Westermann H 2013 Survey on broadband techniques for vibration energy harvesting *J. Intell. Mater. Syst. Struct.* **24** 1291–1302
[8] Gafforelli G, Corigliano A, Xu R and Kim S G 2014 Experimental verification of a bridge-shaped, nonlinear vibration energy harvester *Appl. Phys. Lett.* **105** 203901
[9] Daqaq M F 2012 On intentional introduction of stiffness nonlinearities for energy harvesting under white Gaussian excitations *Nonlinear Dyn.* **69** 1063–79
[10] Erturk A and Inman D J 2011 Broadband piezoelectric power generation on high-energy orbits of the bistable Duffing oscillator with electromechanical coupling *J. Sound Vib.* **330** 2339–53
[11] Harne R L and Wang K W 2013 A review of the recent research on vibration energy harvesting via bistable systems *Smart. Mater. Struct.* **22** 023001
[12] Pellegrini S P, Tolou N, Schenk M and Herder J L 2013 Bistable vibration energy harvesters: a review *J. Intell. Mater. Syst. Struct.* **24** 1303–12
[13] Kim P and Seok J 2014 A multi-stable energy harvester: dynamic modeling and bifurcation

analysis *J. Sound Vib.* **333** 5525–47
[14] Zhou S, Cao J, Inman D J, Lin J, Liu S S and Wang Z Z 2014 Broadband tristable energy harvester: modeling and experiment verification *Appl. Energ.* **133** 33–9
[15] Jung J, Kim P, Lee J and Seok J 2015 Nonlinear dynamic and energetic characteristics of piezoelectric energy harvester with two rotatable external magnets *Int. J. Mech. Sci.* **92** 206–22
[16] Tékam G T O, Kwuimy C A K and Woafo P 2015 Analysis of tristable energy harvesting system having fractional order viscoelastic material *Chaos* **25** 013112
[17] Li H T, Qin W Y, Lan C B, Deng W Z and Zhou Z Y 2016 Dynamics and coherence resonance of tristable energy harvesting system *Smart. Mater. Struct.* **25** 015001
[18] Cook-Chennault K A, Thambi N and Sastry A M 2008 Powering MEMS portable devices-A review of non-regenerative and regenerative power supply systems with special emphasis on piezoelectric energy harvesting systems *Smart. Mater. Struct.* **17** 043001
[19] Gu L and Livermore C 2011 Impact-driven, frequency up-converting coupled vibration energy harvesting device for low frequency operation *Smart. Mater. Struct.* **20** 045004
[20] Stoykov S, Litak G and Manoach E 2015 Vibration energy harvesting by a Timoshenko beam model and piezoelectric transducer *Eur. Phys. J.-Spec. Top.* **224** 2755–70
[21] Halim M A and Park J Y 2014 Theoretical modeling and analysis of mechanical impact driven and frequency up-converted piezoelectric energy harvester for low-frequency and wide-bandwidth operation *Sens. Actuators A, Phys.* **208** 56–65
[22] Deng W and Wang Y 2016 Non-contact magnetically coupled rectilinear-rotary oscillations to exploit low-frequency broadband energy harvesting with frequency up-conversion *Appl. Phys. Lett.* **109** 133903
[23] Wang C, Zhang Q and Wang W 2017 Low-frequency wideband vibration energy harvesting by using frequency up-conversion and quin-stable nonlinearity *J. Sound Vib.* **399** 169–81
[24] Wang C, Zhang Q and Wang W 2017 Wideband quin-stable energy harvesting via combined nonlinearity *AIP Advances* **7** 045314
[25] Griffiths D J 1998 Introduction to Electrodynamics (New Jersey: Prentice Hall)